Dense vertical profiling of the natural magnetic field with a suspended QuSpin QTFM Gen 2 under azimuth-balanced acquisition

Andrew Musinov[1]* | Eugene Podgorbuntsev[1] | Roman Gornov[1]

[1] BlueCap Minerals Pty Ltd, 26 Cimbrook Way, Duncraig, Western Australia 6023, Australia

* Corresponding author: Andrew Musinov · andrew@bluecap.au

ORCID: 0009-0004-0210-5209

Preprint statement
This manuscript is a non-peer-reviewed EarthArXiv preprint. This corrected version is prepared for submission to the *Vietnam Journal of Earth Sciences* and is not under consideration by another journal.

EarthArXiv DOI: 10.31223/X5T789

Research Paper · Four field sites · 204 processed site-height conditions · 25-50 m sensor AGL

Corrected data and code: Zenodo DOI 10.5281/zenodo.22054325

Prepared 22 August 2026 · Field experiment conducted 11 March 2026 · Khanh Hoa, Vietnam

Dense vertical profiling of the natural magnetic field with a suspended QuSpin QTFM Gen 2 under azimuth-balanced acquisition

Andrew Musinov[1]*, Eugene Podgorbuntsev[1], Roman Gornov[1]

[1] BlueCap Minerals Pty Ltd, 26 Cimbrook Way, Duncraig, Western Australia 6023, Australia

* Corresponding author: Andrew Musinov, andrew@bluecap.au

ORCID: https://orcid.org/0009-0004-0210-5209

Abstract

Sensor height is part of the observation geometry of a magnetic survey. We quantified how processed, azimuth-balanced total magnetic field changed with sensor height above ground level (AGL) for a suspended QuSpin QTFM Gen 2 at four agricultural-field sites in Xã Bác Ái Tây, Khánh Hòa, Vietnam. The sensor was suspended 20 m below a geophysical drone helicopter. At each nominal condition from 25.0 to 50.0 m AGL in 0.5 m increments, the freely rotating tubular bird completed 8-12 slow yaw turns. Bird-mounted range LiDAR measured sensor AGL; a stationary QTFM Gen 2 monitored temporal variation; acquisition was nominally 60 Hz; and wind did not exceed 2 m/s. The analysed dataset contains four vertical profiles, each with 51 dependent height conditions.

Relative to the nominal 35 m condition, the processed field differed by +15.8 to +26.7 nT at nominal 25 m and by -6.2 to -10.3 nT at nominal 50 m. The nominal 25-50 m response span was 22.0-37.0 nT, and the local gradient near 35 m was -0.78 to -1.42 nT/m. Linear interpolation to actual LiDAR AGL showed a maximum absolute departure of 0.8 nT within the full physical corridor 34.5-35.5 m. A deterministic inverse-cube benchmark, calculated as A35(35/h)^3 rather than regression-fitted, matched the processed anomaly with RMSE 0.043-0.100 nT. The response magnitude differed among sites, excluding one universal scalar nT/m height correction. Operationally, uncontrolled AGL variation can introduce non-geological field differences large enough to affect line acceptance, levelling and subsequent modelling, whereas physical corridor control reduces this risk at acquisition. The experiment does not directly quantify spatial continuation, map displacement or drill-target error; those require coincident multi-height survey lines or grids.

Keywords: drone magnetometry; scalar atomic magnetometer; sensor height above ground level; magnetic height response; heading compensation; airborne geophysics

1. Introduction

Drone magnetic systems can operate closer to geological sources than conventional crewed aircraft. The reduced source-sensor distance increases sensitivity to short-wavelength field components, but it also increases sensitivity to sensor trajectory, height, orientation and platform-related fields (Kaub et al., 2021; Phelps et al., 2022). Sensor AGL is therefore part of the observation geometry rather than ancillary navigation metadata.

Increasing observation height attenuates short wavelengths more strongly than long wavelengths and broadens local anomalies before levelling, gridding, derivatives or inversion (Ekinci, 2021). Upward continuation is stable but intentionally smooths the field. Downward continuation predicts a field closer to its sources and is ill-conditioned because high-frequency measurement and geometry errors are amplified unless the solution is regularised (Cooper, 2004; Zuo et al., 2020). Equivalent-source approaches can represent irregular observation surfaces, but their output depends on source parameterisation and regularisation (Gavazzi et al., 2020). Consequently, retaining actual sensor AGL and acquiring a narrow physical height corridor are direct controls on data comparability.

This issue has an immediate commercial consequence. When terrain following is poor, adjacent observations or lines can contain geometry-induced magnetic differences that are unrelated to lateral geology. Such differences can increase levelling effort, destabilise grids and inversions, trigger line rejection or require a costly re-flight. Mathematical height correction remains valuable, but it is downstream risk control rather than a substitute for controlling the observation geometry during acquisition.

Orientation-dependent response is a second control on suspended atomic magnetometry. Repeated full-azimuth coverage allows the angle-independent component to be separated from periodic heading terms. Published drone aeromagnetic work has shown the importance of installed-system compensation and repeat acquisition (Phelps et al., 2022; Wang et al., 2020). In the present experiment, 8-12 slow yaw turns were acquired at every height condition, and the published analytical input is the processed azimuth-balanced condition mean.

The study addresses one deliberately narrow question: how does a processed total-field observation at a nominal hover site change as physical sensor AGL changes? Four vertical profiles, each containing 51 nominal height conditions, were used to test whether (H1) the processed field changes monotonically with height, (H2) response magnitude differs among sites, (H3) the physical 34.5-35.5 m corridor materially limits pointwise height-associated differences, and (H4) a deterministic inverse-cube calculation provides a useful benchmark without implying a universal law. The results support all four propositions within the limitations of ascending-only, condition-level vertical profiles.

2. Background and field setting

2.1. Sites

The experiment was conducted on 11 March 2026 at four separate agricultural-field sites near Bậc Ray Một and Phước Bình, Xã Bác Ái Tây, Khánh Hòa, Vietnam. Coordinates are WGS 84.

Site	Latitude	Longitude	Decimal degrees	Locality
A	11°59'59.54" N	108°49'00.11" E	11.9998722, 108.8166972	Bậc Ray Một / Phước Bình
B	12°00'23.31" N	108°49'07.11" E	12.0064750, 108.8186417	Bậc Ray Một / Phước Bình
C	12°00'46.07" N	108°49'15.44" E	12.0127972, 108.8209556	Bậc Ray Một
D	12°00'58.49" N	108°48'51.74" E	12.0162472, 108.8143722	Bậc Ray Một / Phước Bình

The sites were open fields away from buildings and without a deliberately emplaced magnetic target. A known artificial source was unnecessary because the objective was to characterize the installed system in the spatially varying natural field encountered during survey operations. This condition does not imply the absence of geological sources or local crustal gradients.

2.2. Weather and reference height

Flights were scheduled for calm conditions. Wind was measured with a Kestrel 5500 with LiNK and did not exceed 2 m/s during the four experiments. Low wind reduced irregular pendulum motion and supported slow free yaw rotation.

BlueCap uses 35 m sensor AGL as a lower operational and safety reference for the class of valley surveys considered here, where trees and isolated canopy or obstacle features can rise above surrounding terrain. The complete one-metre experimental compliance corridor is 34.5-35.5 m. Higher sensor AGL may be required for obstacle clearance and remains valid as a different observation geometry. The 35 m value is an operational rule for this survey context, not a universal safe height for all terrain, vegetation or aviation conditions.

3. Material and methods

3.1. Airborne magnetometer and suspended bird

The airborne sensor was a QuSpin QTFM Gen 2 scalar total-field atomic magnetometer installed in a suspended bird. The aerodynamic wings were removed for the experiment, leaving a predominantly tubular body that could rotate about the near-vertical suspension axis. The bird was connected to the BlueCapHeli by a pre-measured 20 m line.

The scalar zero-crossing count was set to SZC/ZC = 100. QuSpin identifies this as the Average magnetic-environment profile, intermediate between Noisy = 40 and Quiet = 200. A larger zero-crossing count favours sensitivity in a quiet field, whereas a smaller value increases tolerance to magnetic noise and motion (QuSpin, 2026a, 2026b). All programmable onboard digital filters were Off. Thus the QTFM 50/60 Hz notch and programmable low-pass, high-pass and custom filters did not shape the acquired output (QuSpin, 2026c). Downstream condition averaging is distinct from these onboard filters.

Published manufacturer specifications give typical QTFM Gen 2 scalar sensitivity of approximately 3 pT/sqrt(Hz) and uncompensated heading error below 3 nT (QuSpin, 2026d). These standalone specifications do not represent installed survey noise and are not outcomes of the present condition-level analysis.

3.2. Carrier, positioning and height channels

BlueCapHeli is a 25 kg-class single-rotor petrol drone helicopter developed and operated as a carrier for magnetic, LiDAR, radiometric and imaging surveys (BlueCap, 2026a). Helicopter height was controlled using BlueCapRTK (BlueCap, 2026b). A nominal height condition was accepted only after a stable RTK fixed solution and a reported vertical solution accuracy of 0.005 m were achieved. This threshold describes the navigation acceptance criterion for the carrier; it is not a claim of 5 mm absolute position accuracy for the suspended QTFM.

Carrier coordinates and sensor coordinates were not treated as identical. The bird-mounted GNSS directly observed the sensor assembly, while carrier RTK, suspension length, bird IMU/heading, range LiDAR, measured wind and the aerodynamic response model supplied additional kinematic constraints and quality-control channels. This multisensor geometry prevents centimetre-scale carrier RTK performance from being misreported as identical sensor-position accuracy. The present analysis uses the processed LiDAR AGL associated with each magnetic condition mean; it does not estimate a new horizontal trajectory from the public workbook.

The range LiDAR was mounted on the bird and measured distance to the surface. Actual sensor AGL was obtained from LiDAR with the recorded attitude and surface geometry. The achieved condition-level AGL statistics reported below are derived from the processed workbook and supersede any assumption that carrier RTK accuracy alone describes sensor height accuracy.

3.3. Ground magnetic reference

A second QTFM Gen 2 was installed on the ground approximately 35 m horizontally from the projection of the suspended sensor. It continuously monitored temporal magnetic-field variation during each flight. Correction used the temporal departure of the base record from a selected reference epoch rather than subtracting its entire absolute level, which would mix diurnal variation with local gradient, height difference and inter-instrument offset.

3.4. Experimental procedure

At take-off, an initial yaw impulse was applied to the stripped tubular bird. The bird then rotated freely. The helicopter increased height sequentially while the bird-mounted LiDAR monitored sensor AGL. Only an ascending order was used.

Andrew Musinov conducted the field investigation, piloted the drone and supervised acquisition in Vietnam. Eugene Podgorbuntsev and Roman Gornov did not participate onsite; they received the acquired results for geophysical processing, data curation, analysis and validation.

Each site followed the same nominal program:

1. start at 25.0 m sensor AGL;
2. acquire at 0.5 m increments;
3. finish at 50.0 m sensor AGL;
4. retain 8-12 complete slow yaw turns at each level; and
5. record QTFM and synchronized instrumentation at a nominal 60 Hz.

The complete sequence contains 51 nominal height conditions per site and approximately 408-612 rotations per flight. Across four sites this corresponds to 204 site-height conditions and approximately 1632-2448 rotations. Individual rotations are acquisition controls, not independent statistical replicates in this paper. Each flight lasted approximately 95-105 min.

Because all levels were acquired upward, height is correlated with elapsed time, fuel or power state, electronic temperature and possible changes in yaw rate. The simultaneous base station constrains temporal geomagnetic variation but cannot remove every time-height confounder. A repeated experiment should randomize, descend, or otherwise balance height order.

3.5. Synchronization and temporal correction

Instrument channels were placed on a common UTC timeline while retaining native timestamps. The stationary QTFM record was used to remove temporal departure from its selected reference level rather than its absolute field value. The correction is represented by

$$T\_dc(t) = T\_air(t) - [T\_base(t) - T\_base(t\_ref)],$$

where T_air is airborne total field, T_base is ground total field, and t_ref is the base reference epoch. The public workbook begins with processed condition means and does not expose the 60 Hz base trace; the temporal-correction result is therefore an upstream processing input to this condition-level study.

3.6. Height conditions and azimuth-balanced estimates

Height plateaus were identified from LiDAR AGL and event or flight channels. Actual height statistics were associated with each nominal level. Yaw was unwrapped to identify complete rotations, and transition segments between levels were excluded from the condition estimates.

At site s and height h, the corrected magnetic record was represented during processing by a harmonic nuisance model:

$$T\_dc,s,h(t) = beta\_0,s,h + sum[k=1..K] \{a\_k,s,h \cos[k\ psi(t)] + b\_k,s,h \sin[k\ psi(t)]\} + epsilon(t),$$

where beta_0 is the angle-independent condition estimate, a_k and b_k are periodic heading coefficients, psi is yaw, K is the processing model order, and epsilon contains residual motion, magnetic and timing effects. The public condition-level dataset contains the resulting processed mean_total_field_nT values, not the 60 Hz samples, individual-turn estimates or harmonic coefficients. Accordingly, this paper analyses the height response of those condition means and does not independently re-estimate heading-model uncertainty.

3.7. Height-response quantities

For each site, pointwise height response was expressed relative to the nominal 35 m condition:

$$Delta\ T\_s(h) = beta\_0,s(h) - beta\_0,s(35\ m).$$

The local gradient near 35 m was calculated by a central difference between the nominal 34.5 and 35.5 m conditions using their measured AGL values. Additional metrics were target-versus-measured AGL RMSE and the response span across the nominal 25-50 m target conditions. To evaluate the physical 34.5-35.5 m corridor, total field was linearly interpolated against measured LiDAR AGL to 34.5, 35.0 and 35.5 m separately for each site. Because the published AGL values are rounded to 0.1 m and no within-condition dispersion is available, corridor results are reported to 0.1 nT.

The inverse-cube benchmark was calculated, not statistically fitted:

$$predicted\_r3\_s(h) = A35\_s\ (35/h)^3,$$

where h is nominal height target in metres and A35 is 12, 9, 15 and 11 nT for Sites A-D, respectively. Benchmark RMSE was calculated consistently from corrected_anomaly_nT minus predicted_r3_anomaly_nT across the 51 conditions at each site. The compact-source form is retained as a physical benchmark; it is not imposed as a universal law for a distributed natural field.

The experiment comprises four site profiles. The 51 height conditions within a profile are dependent observations, not 51 independent experimental replicates. Raw 60 Hz noise, individual-turn repeatability, harmonic uncertainty, invalid/dead-zone fraction, spatial spectra and crossover statistics are outside the released dataset and are not inferred from the smooth condition-level curves.

4. Results

4.1. Experimental coverage

All four profiles contain 51 processed nominal height conditions from 25.0 to 50.0 m. Actual condition-level LiDAR AGL differed from the nominal target by 0.08-0.09 m RMSE among sites. These values quantify target compliance of the published condition means; they do not represent within-condition height scatter.

4.2. Processed pointwise height response

The processed field decreased monotonically with increasing nominal height at all four sites, but its magnitude and local gradient differed (Table 1; Figure 1). At the nominal 25 m condition, Delta T was +15.8 to +26.7 nT. At the nominal 50 m condition, Delta T was -6.2 to -10.3 nT. The response span across nominal 25-50 m conditions was 22.0 nT at Site B and 37.0 nT at Site C.

Table 1. Site-level processed height-response metrics.

Site	T at nominal 35 m (nT)	Delta T, nominal 25 m (nT)	Delta T, nominal 50 m (nT)	dT/dh near 35 m (nT/m)	AGL target RMSE (m)	Nominal response span (nT)	RMSE vs calculated 1/r^3 (nT)
A	41,924.0	+21.3	-8.2	-1.21	0.08	29.5	0.045
B	41,931.3	+15.8	-6.2	-0.78	0.08	22.0	0.052
C	41,926.2	+26.7	-10.3	-1.42	0.08	37.0	0.100
D	41,937.4	+19.3	-7.6	-0.92	0.09	26.9	0.043

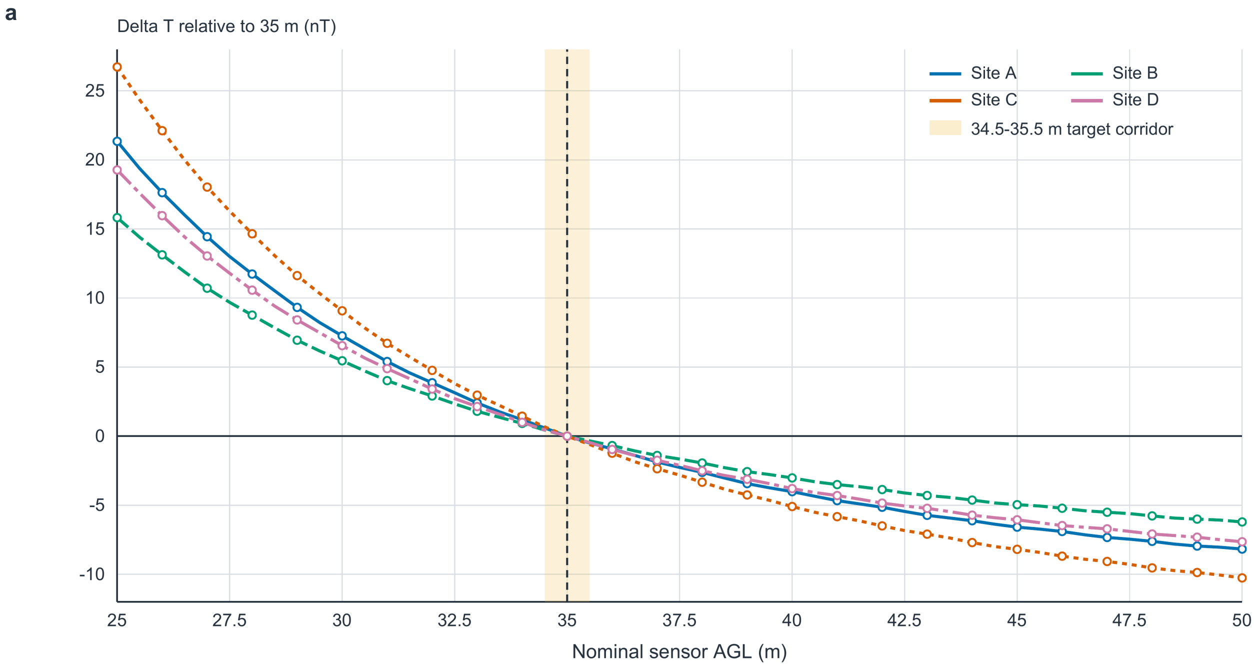

Figure 1. Processed pointwise height response at four sites. Delta T is referenced independently to the nominal 35 m condition at each site. The gold band marks the full 34.5-35.5 m operational corridor. Each curve contains 51 condition-level observations at 0.5 m nominal spacing.

The magnitude of the local gradient differed by approximately 1.8 times between Sites B and C. The four profiles therefore exclude a single site-independent scalar nT/m correction across the observed locations.

4.3. Physical operational corridor

Linear interpolation to measured LiDAR AGL produced maximum absolute departures within the physical 34.5-35.5 m corridor of 0.6, 0.4, 0.8 and 0.5 nT at Sites A-D, respectively. The largest corridor-boundary value was 0.8 nT at Site C. By comparison, nominal conditions 5 m below and above 35 m differed by +5.5 to +9.1 nT at 30 m and by -3.0 to -5.1 nT at 40 m. The broad 25-50 m programme produced differences of tens of nanotesla.

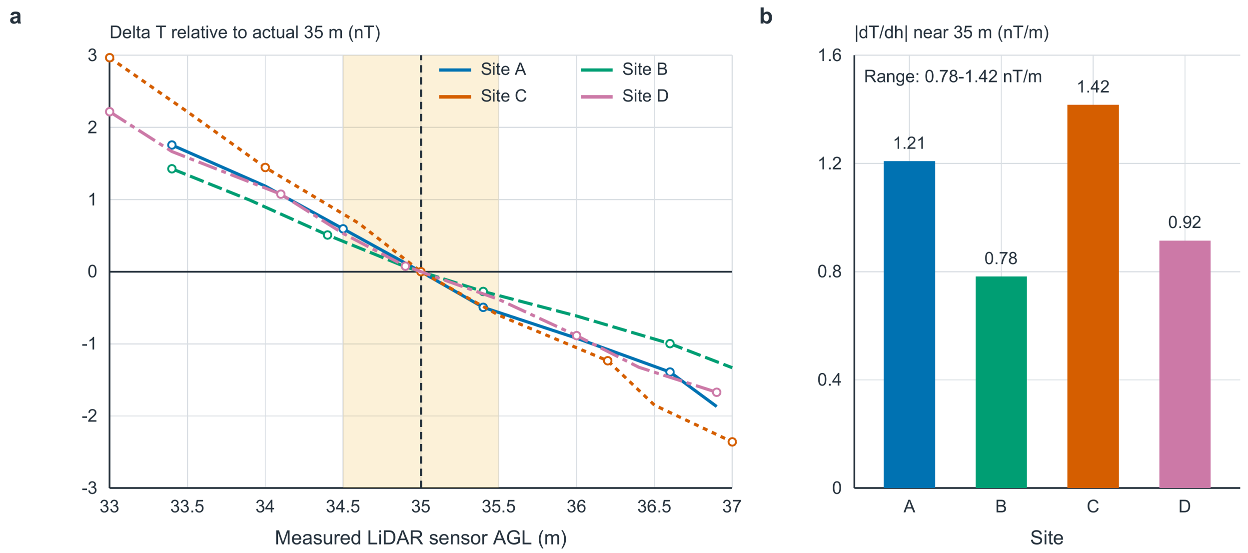

Figure 2. (a) Processed response near the nominal 35 m reference, with the complete 34.5-35.5 m physical corridor highlighted. (b) Absolute local gradient calculated from measured AGL at conditions bracketing 35 m. Corridor-boundary values are separately interpolated to actual AGL in the released workbook.

Target-versus-measured AGL RMSE was 0.08-0.09 m. The physical-corridor result is commercially important because it constrains acquisition-induced variation at the point of measurement, whereas excursions of several metres generated differences one to two orders of magnitude larger.

4.4. Calculated inverse-cube benchmark

The deterministic A35(35/h)^3 benchmark matched corrected_anomaly_nT with site-level RMSE of 0.043-0.100 nT (Figure 3). It was calculated directly from the stated formula and fixed site anchors and was not regression-fitted to minimise RMSE. The result demonstrates that a compact-source inverse-cube form is an effective numerical description of these processed profiles. It remains a benchmark rather than proof that every distributed natural source obeys the same law.

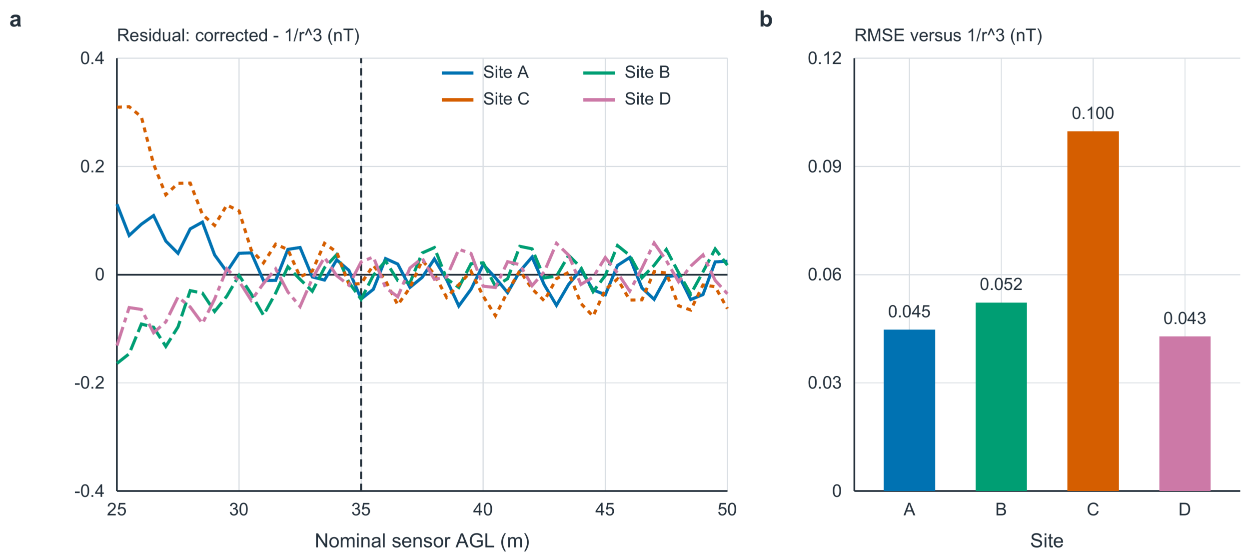

Figure 3. (a) Residual corrected_anomaly_nT minus the calculated nominal-height A35(35/h)^3 benchmark. (b) Site-level RMSE of the same residual definition.

5. Discussion

5.1. What the experiment establishes

The four vertical profiles establish a strong monotonic height-associated relationship in the processed azimuth-balanced field of the installed QTFM Gen 2 system. All sites show the same direction of change, while response magnitude differs materially. The condition-level evidence therefore supports H1-H3 within this acquisition protocol. It does not estimate between-flight repeatability because each site was profiled once.

The experiment also shows why sensor AGL should remain attached to every accepted magnetic observation. A height excursion can produce a field change before any geological processing begins. If geometry changes are not retained and classified, they can be interpreted silently as spatial geology during levelling, gridding or inversion.

For client-facing quality control, three acquisition states should be distinguished:

1. **Compliant acquisition:** actual sensor AGL lies within 34.5-35.5 m.
2. **Deliberately higher acquisition:** height is increased for safety or obstacle clearance and retained as a different observation geometry.
3. **Unplanned excursion:** departure from the target corridor is recorded by LiDAR and reviewed for acceptance, re-flight or interpretation impact.

An out-of-corridor observation is not automatically unusable. Its comparability depends on local geology, trajectory quality and the assumptions of subsequent height modelling. However, the measured 22.0-37.0 nT profile spans show that broad AGL variation can create differences far above sub-nanotesla survey precision objectives. In production this can appear as line-to-line inconsistency, increase levelling and interpretation effort, cause QC rejection, and require re-flight. Because re-mobilisation and a replacement survey day can cost tens of thousands of dollars, physical AGL control is a commercially material prevention measure. The four different slopes also show why one universal Delta T-per-metre correction cannot replace acquisition control.

5.2. Interpretation boundary

Vertical hover profiles measure how one point observation changes with height. They do not measure lateral anomaly broadening, attenuation of individual wavenumbers along a line, or equivalence between a continued field and a physical observation on the target surface. Those claims require coincident horizontal lines or grids acquired physically at multiple sensor heights. A continuation study should compare real 25 or 30 m lines upward-continued to 35 m, and real 40, 45 or 50 m lines downward-continued to 35 m, against a physically acquired 34.5-35.5 m reference.

For the same reason, the present study does not assign a numerical displacement to a 2D map, 3D inversion or drill target. It provides the preceding field evidence: changing observation height is associated with a material change in the processed magnetic value, and the magnitude is location dependent. Downstream effects on anomaly geometry, inferred source depth or planned drill intercept require the spatial experiment.

5.3. Installed noise and comparison with other sensors

Smooth condition means are not measurements of intrinsic noise floor or installed survey noise. This dataset cannot yield amplitude spectral density, fourth-difference noise, raw standard deviation, turn-to-turn repeatability, line-to-line noise or residual heading error. It therefore does not demonstrate that QTFM Gen 2 is quieter than Geometrics MagArrow II.

Manufacturer specifications provide context only. QTFM Gen 2 lists typical scalar sensitivity near 3 pT/sqrt(Hz) and uncompensated heading error below 3 nT (QuSpin, 2026d), whereas the MagArrow II sheet lists typical noise or sensitivity of 5 pT/sqrt(Hz) and typical heading error of +/-5 nT over a full rotation (Geometrics, 2023). The values arise from different instruments, procedures and bandwidth conventions. A defensible comparison requires coincident lines, common bandwidth and timing, the same physical AGL, PSD or ASD, fourth differences, crossover statistics and blind comparison of final maps.

The installed configuration has explicit trade-offs. SZC/ZC = 100 favours robustness over the maximum quiet-field sensitivity of SZC = 200. Filters Off preserves broadband output and avoids onboard phase or amplitude shaping, but leaves mains, platform and high-frequency components for downstream treatment. The 20 m suspension reduces carrier magnetic influence while increasing the need for trajectory reconstruction and pendulum control. Ascending-only acquisition does not test order hysteresis.

6. Conclusions

1. Four vertical site profiles, each containing 51 dependent conditions, showed monotonic processed field change across nominal target heights 25-50 m. Relative to the nominal 35 m condition, Delta T was +15.8 to +26.7 nT at nominal 25 m and -6.2 to -10.3 nT at nominal 50 m.
2. Response magnitude differed among the four sites. The nominal-condition span was 22.0-37.0 nT and the local gradient near 35 m was -0.78 to -1.42 nT/m, excluding one universal scalar nT/m correction.
3. Target-versus-measured LiDAR AGL RMSE was 0.08-0.09 m. Linear interpolation to the physical 34.5-35.5 m corridor produced maximum absolute departures of 0.4-0.8 nT from actual 35 m.
4. The calculated inverse-cube benchmark achieved RMSE 0.043-0.100 nT. It is a strong deterministic description of the processed anomaly profiles, but not a universal law for distributed geological sources.
5. Commercially, broad AGL variation can introduce non-geological differences large enough to complicate line acceptance, levelling, gridding and inversion and to cause expensive re-flight. Continuous sensor-mounted LiDAR, physical corridor control and immediate field QC are therefore primary data-quality controls.
6. Coincident horizontal lines or grids at multiple physical heights remain necessary to quantify continuation error, map displacement, inversion bias and drill-target consequences.

CRediT authorship contribution statement

Andrew Musinov: Conceptualization, Methodology, Investigation, drone piloting, field acquisition, Resources, Project administration, Supervision, Writing - original draft, Writing - review and editing. Eugene Podgorbuntsev: Formal analysis, Data curation, Validation, Visualization, Writing - review and editing. Roman Gornov: Formal analysis, Data curation, Validation, Visualization, Writing - review and editing. Andrew Musinov alone conducted and piloted the Vietnam field programme; Eugene Podgorbuntsev and Roman Gornov received and processed the results and did not participate onsite.

Funding

This research received no external funding. BlueCap Minerals Pty Ltd supplied the instruments, aircraft, personnel, field logistics, processing resources and publication preparation. As the employer and internal sponsor of the authors, BlueCap participated in study design, data collection, analysis, interpretation, writing and the decision to prepare the work for publication.

Declaration of competing interest

All authors are affiliated with BlueCap Minerals Pty Ltd. Andrew Musinov is the company's Managing Director. BlueCap Minerals Pty Ltd develops and operates the geophysical carrier and suspended-bird systems discussed in this study and therefore has a commercial interest in the operational application of the reported results.

Data and code availability

The corrected processed data, site coordinates, explicit inverse-cube calculation, actual-AGL corridor interpolation and figure-generation code are openly available from Zenodo at https://doi.org/10.5281/zenodo.22054325. Proprietary control implementations and operationally restricted records are excluded from the public package. The public analytical unit is the processed site-height condition, not the raw 60 Hz, individual-turn, IMU or base-station time series.

Declaration of generative AI and AI-assisted technologies

OpenAI Codex was used solely to assist with manuscript structuring. The authors take full responsibility for the final content.

Acknowledgements

The authors thank Phan Thị Minh, Vietnam Operations Director, for operational coordination in Vietnam, and the BlueCap field operations and data engineering personnel who supported equipment preparation and the field programme.

References

BlueCap, 2026a. BlueCapHeli: long-endurance petrol drone helicopter for geophysical surveys. https://bluecap.au/survey-equipment/bluecapheli-gasoline-helicopters-long-endurance-australia/ (accessed 22 August 2026).

BlueCap, 2026b. BlueCapRTK geodetic drone RTK positioning. https://bluecap.au/survey-equipment/bluecaprtk-geodetic-drone-rtk-positioning/ (accessed 22 August 2026).

Cooper, G., 2004. The stable downward continuation of potential field data. *Exploration Geophysics* 35(4), 260-265. https://doi.org/10.1071/EG04260.

Ekinci, Y.L., 2021. On the drape and level flying aeromagnetic survey modes with terrain effects, and data reduction between arbitrary surfaces. *Turkish Journal of Earth Sciences* 30(3), 409-424. https://doi.org/10.3906/yer-2007-18.

Gavazzi, B., Bertrand, L., Munschy, M., Mercier de Lépinay, J., Diraison, M., Géraud, Y., 2020. On the use of aeromagnetism for geological interpretation: 1. Comparison of scalar and vector magnetometers for aeromagnetic surveys and an equivalent source interpolator for combining, gridding, and transforming fixed altitude and draping data sets. *Journal of Geophysical Research: Solid Earth* 125(5), e2019JB018870. https://doi.org/10.1029/2019JB018870.

Geometrics, 2023. MagArrow II drone-deployable magnetometer specifications. https://www.geometrics.com/wp-content/uploads/2023/08/MagArrow_II_UAS_SpecSheet_07212023.pdf (accessed 22 August 2026).

Kaub, L., Keller, G., Bouligand, C., Glen, J.M.G., 2021. Magnetic surveys with unmanned aerial systems: software for assessing and comparing the accuracy of different sensor systems, suspension designs and compensation methods. *Geochemistry, Geophysics, Geosystems* 22(7), e2021GC009745. https://doi.org/10.1029/2021GC009745.

Phelps, G., Bracken, R.E., Spritzer, J., White, D.S., 2022. Achieving sub-nanoTesla precision in multirotor UAV aeromagnetic surveys. *Journal of Applied Geophysics* 206, 104779. https://doi.org/10.1016/j.jappgeo.2022.104779.

QuSpin, 2026a. QTFM Gen 2 sensor configuration. https://quspin.com/qtfm-gen-2/qtfm-gen-2-user-guide/sensor-configuration/ (accessed 22 August 2026).

QuSpin, 2026b. QTFM Gen 2 configuration profiles. https://quspin.com/qtfm-gen-2/qtfm-gen-2-user-guide/qtfm2-sensor-profile-configuration/ (accessed 22 August 2026).

QuSpin, 2026c. QTFM Gen 2 quick reference: serial commands and filters. https://quspin.com/qtfm-gen-2-quick-reference/ (accessed 22 August 2026).

QuSpin, 2026d. QTFM Gen 2 scalar total-field magnetometer. https://quspin.com/qtfm-gen-2/ (accessed 22 August 2026).

Wang, H., Du, C., Wang, H., Xia, M., Peng, X., Guo, H., 2020. Aeromagnetic compensation with suppressing heading error of the scalar atomic magnetometer. *IEEE Geoscience and Remote Sensing Letters* 17(7), 1134-1138. https://doi.org/10.1109/LGRS.2019.2940824.

Zuo, B., Hu, X., Leão-Santos, M., Wang, L., Cai, Y., 2020. Downward continuation and transformation of total-field magnetic anomalies into magnetic gradient tensors between arbitrary surfaces using multilayer equivalent sources. *Geophysical Research Letters* 47(16), e2020GL088678. https://doi.org/10.1029/2020GL088678.